Journal of Southeast University (English Edition) Vol. 36, No. 1, pp. 56 - 66 Mar. 2020 ISSN 1003—7985

Higher mode effects in hinged wall with BRBs in base-frame structures using distributed parameter models

Yang Xiaoyan[1] Wu Jing[1] Pang Xixi[2] Wang Qiang[3] Zhang Meng[4]

([1]Key Laboratory of Concrete and Prestressed Concrete Structures of Ministry of Education, Southeast University, Nanjing 211189, China)
([2]Xuzhou Survey and Design Center, State Grid Economic and Technological Research Institute Co., Ltd., Xuzhou 221005, China)
([3]Hong Kong Huayi Design Consultants (Shenzhen) Ltd., Shenzhen 518057, China)
([4]Baosheng Integrated System Technology Co. Ltd., Baoying 225000, China)

Abstract: To investigate the effect of higher modes on the displacement and inner forces in HWBB (hinged wall with buckling-restrained braces in base)-frame structure, distributed parameter models for both the HWBB-hinged frame structure and the HWBB-MRF (moment resisting frame) structure are built. The hinged wall is simplified as a flexural beam. BRBs (bucking-restrained braces) are simplified to a rotational spring. MRF is simplified to a shear beam. Vibration equations of distributed parameter models are derived. Natural periods, natural modes of vibration, inner forces and displacements of the distributed parameter models are derived based on the vibration equations using numerical methods. The effect of the relative stiffness ratio and the rotational stiffness ratio on the higher mode effects is investigated. For elastic structures, the global displacement and shear in MRF are predominantly controlled by the first mode, while the shear and bending moment in the wall are significantly affected by higher mode effects. The effect of the yielding of BRB on the inner forces distribution in the HWBB-hinged frame is investigated. The results indicate that the first mode will no longer contribute to the inner forces and the contribution from higher modes to inner forces increases after the BRBs yield. Displacement is not sensitive to higher mode effects and it is controlled by the first mode after the BRBs yield. Parameter analysis demonstrates that the displacement amplitudes are reduced with the increase in the flexural stiffness of the wall before the flexural stiffness reaches a certain value. The first three periods decrease with the increase in the rotational stiffness. With the increase in the rotational stiffness ratio, the contribution from the first mode decreases while contributions from both the second mode and third mode increase.

Key words: hinged wall; higher mode effects; flexural beam; rotational spring; rotational stiffness ratio
DOI: 10.3969/j.issn.1003-7985.2020.01.008

Received 2019-09-25, **Revised** 2019-12-26.

Biographies: Yang Xiaoyan (1990—), female, Ph. D. candidate; Wu Jing (corresponding author), male, doctor, professor, seuwj@seu.edu.cn.

Foundation items: The National Key Research and Development Program of China (No. 2018YFC0705802), the National Natural Science Foundation of China (No. 51978165), the Fundamental Research Funds for the Central Universities (No. 3205007720), Postgraduate Research and Practice Innovation Program of Jiangsu Province (No. 3205007720).

Citation: Yang Xiaoyan, Wu Jing, Pang Xixi, et al. Higher mode effects in hinged wall with BRBs in base-frame structures using distributed parameter models[J]. Journal of Southeast University (English Edition), 2020, 36(1): 56 - 66. DOI: 10.3969/j.issn.1003-7985.2020.01.008.

Hinged walls or rocking cores can control the deformation pattern of the frame due to their large flexural stiffness and avoid weak story failure in frame structures. Alavi et al.[1] strengthened multi-story frame structures with hinged walls, which effectively reduced the drift demands. Wada et al.[2-4] used pin-supported walls to retrofit an existing SRC frame structure. The distributions of interstory drift ratios were improved by adding pin-supported walls. A pivoting core wall, which was supported on a friction pendulum bearing and can pivot about its base, was used to retrofit a steel moment frame building. The weak story failure was eliminated[5].

The lateral stiffness of hinged walls is zero and the structural responses cannot be reduced by adding hinged walls. Qu et al.[4] concluded that the magnitude of interstory drift ratios was not reduced by adding pin-supported walls. Makris et al.[6] showed that the pinned wall can increase the displacement response of the moment resisting frame. Therefore, dampers are added to the hinged walls to provide stiffness to them and dissipate seismic energy. Interstory drift ratios were reduced by adding dampers between the pin-supported walls and the original SRC columns[4]. BRBs were installed between the steel moment frame and the pivoting core wall to dissipate seismic energy[5]. The hinged wall contains both a steel truss and a concrete wall, which is composed of precast wall panels connected by pre-stressed tendons[7]. A steel truss which has a large stiffness can also be used as a hinged truss to control the deformation pattern of the structure. Takeuchi et al.[8-11] proposed a spine frame which rotates around the bottom middle point, and buckling restrained columns (BRCs) were used to dissipate seismic energy. A rocking steel shear wall installed with a double acting ring spring system to dissipate energy was investigated[12]. Du et al.[13] investigated the stiffness demand of a light energy dissipative rocking frame that contains self-centering energy dissipative bracing systems to dissipate seismic energy and reduce residual displacement.

Higher mode effects on the bending moment distribution of hinged walls were investigated[14-15], which showed that higher mode effects have to be considered in the design of hinged walls. The rocking wall is simplified as a flexural beam, and dampers installed at the bottom

and between the rocking wall and moment frame are simplified as springs. The preliminary design method of the rocking-wall moment frame is proposed[16–18]. Nima et al.[19] proposed the equations which are used to simplify a rocking truss as a flexural beam. Wu et al.[15] proposed a simplified model for pin-supported wall structures and demonstrated that higher mode effects have to be considered when determining the strength demand of the wall. Moreover, Wiebe et al.[20] derived the vibration equations for a shear beam with a rotational spring at the bottom and a flexural beam with a rotational spring at the bottom. Yang et al.[21] proposed the seismic intensity superposition method to calculate the bending moment demand in the hinged wall considering higher mode effects.

The hinged wall with BRBs in base (HWBB) consists of a hinged wall with replaceable BRBs installed vertically at the bottom of the hinged wall. During a small earthquake, BRBs remain elastic and provide stiffness for HWBB, while BRBs yield under a large earthquake to dissipate seismic energy and provide damping for the structure. The hinged wall remains elastic while BRBs dissipate seismic energy and only BRBs need to be replaced after earthquake, avoiding the toe crushing and yielding of edge bars in conventional shear walls. BRBs provide the flexural strength while the pin bearing provides the shear strength to realize the separation of the load bearing[22]. A pseudo-dynamic test and quasi-static test on a 1∶3 scale three-story hinged truss with BRBs in base (HTBB) were performed to investigate the seismic capacity and seismic performance of the specimen[23]. The hinged truss made up of steel beams, columns and braces can remain elastic during the experiment, while BRBs yielded and dissipated seismic energy. As damage is concentrated in BRBs, only BRBs need to be replaced to restore the function of the specimen. After the consecutively exciting of a minor earthquake, a design earthquake and a strong earthquake, the HTBB specimen withstood 19 cycles of displacement amplitude corresponding to 2.5% roof drift ratio with stable hysteretic performance. This test verified the excellent seismic performance of the HTBB. The hinged wall is able to remain elastic by capacity design which considers higher mode effects to control the deformation pattern of the structure.

The HWBB is applied to frame structures to improve the distribution of displacements and work as the lateral force resisting system. In this study, both the HWBB-hinged frame and HWBB-MRF (moment resisting frame) are analyzed. For the HWBB-hinged frame, as the hinged frame bears no lateral load, the derivation equations concern HWBB with mass distributed along the full height of HWBB and the hinged frame is not included in the simplified model. Vibration equations for these two simplified models are derived. Natural periods and natural modes of vibration are derived. Higher mode effects on structural responses, such as inner forces and displacements, are investigated for both the elastic structure and the plastic HWBB-hinged frame structure where BRBs yield. Parametric studies are conducted to investigate the influence of the relative stiffness ratio and the rotational stiffness ratio on the higher mode effects.

1 Derivation

The simplified model of the HWBB-hinged frame is shown in Fig. 1. Shear deformation of the wall is ignored as the height of the structure is great enough. BRBs offer the whole moment resistance for the structure. BRBs are simplified as a rotational spring. The hinged wall is simplified as a flexural beam with a pinned end. The flexural stiffness of the flexural beam is EI. The rotational stiffness of the rotational spring is denoted as k_b and H denotes the length of the flexural beam.

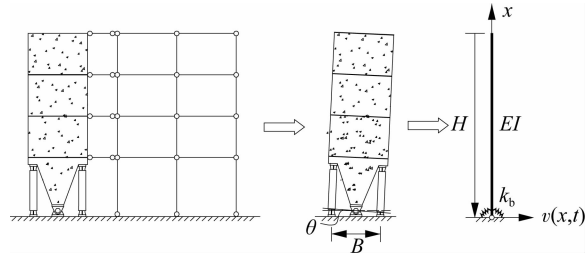

Fig. 1 Simplified model of the HWBB-hinged frame structure

The moment resistance offered by the rotational spring in the simplified model is expressed as

$$M = k_b\theta \tag{1}$$

where θ denotes the interstory drift ratio of the first story, which is caused by the rotation of the hinged wall and it is calculated by the deformation of BRB as follows:

$$\theta = \frac{\Delta u_{BRB}}{0.5B} = \frac{2\varepsilon_{BRB} l_{BRB}}{B} \tag{2}$$

where ε_{BRB} denotes the strain in BRB; l_{BRB} is the length of BRB; Δu_{BRB} is the deformation of BRB; and B is the distance between centerlines of BRBs. Substituting Eq. (2) into Eq. (1) gives

$$k_b = \frac{M}{\theta} = f_{BRB} AB \frac{B}{2\varepsilon_{BRB} l_{BRB}} = \frac{EAB^2}{2l_{BRB}} \tag{3}$$

where A denotes the area of the core plate in BRB and E is the elastic modulus of steel. Vibration equations for the simplified models of both the HWBB-hinged frame and the HWBB-MRF are derived in the following sections.

1.1 HWBB-hinged frame

As shown in Fig. 1, the mass per unit length along the flexural beam is $\bar{m}$. $v(x, t)$ is the transverse-displacement response. Physical properties are distributed evenly along the flexural beam. As the mass and stiffness are evenly

distributed along the flexural beam, the partial differential equation contains only two variables, time and the distance to the bottom of the flexural beam. The partial differential equation of the flexural beam can be expressed as[24]

$$\frac{\partial^4 v(x,t)}{\partial x^4}+\frac{\bar{m}}{EI}\frac{\partial^2 v(x,t)}{\partial t^2}=0 \tag{4}$$

where the second part of the above equation is the inertia force.

Assume that the solution is as follows according to the separation of variables:

$$v(x,t)=\phi(x)\,Y(t) \tag{5}$$

Substituting Eq. (5) into Eq. (4) gives

$$\frac{EI}{\bar{m}}\frac{1}{\phi(x)}\frac{\mathrm{d}^4\phi(x)}{\mathrm{d}x^4}=\omega^2 \tag{6}$$

where ω is the natural circular frequency of the model.

For brevity, define

$$a^4=\frac{\bar{m}\omega^2}{EI} \tag{7}$$

The general solution of Eq. (6) is

$$\phi(x)=A_1\sin ax+A_2\cos ax+A_3\sinh ax+A_4\cosh ax \tag{8}$$

Define the following parameter for brevity:

$$m=\frac{k_\mathrm{b}}{EIa} \tag{9}$$

Four boundary conditions at the ends of the flexural beam are

When $x=0$, $M(0)=k_\mathrm{b}\theta(x=0)$,

$$M(0)=EI\frac{\mathrm{d}^2 v}{\mathrm{d}x^2}(x=0)=k_\mathrm{b}\theta(x=0)=k_\mathrm{b}\frac{\mathrm{d}v}{\mathrm{d}x}(x=0) \tag{10}$$

where M is the bending moment in the wall and θ denotes the rotation of the beam section. Therefore,

$$m(A_1+A_3)=-A_2+A_4 \tag{11}$$

When $x=0$, $\phi(0)=0$,

$$A_2+A_4=0 \tag{12}$$

When $x=L$, $M(L)=0$,

$$-A_1a^2\sin aL-A_2a^2\cos aL+A_3a^2\sinh aL+A_4a^2\cosh aL=0 \tag{13}$$

When $x=L$, $V(L)=0$,

$$-A_1a^3\cos aL+A_2a^3\sin aL+A_3a^3\cosh aL+A_4a^3\sinh aL=0 \tag{14}$$

To obtain a nontrivial solution for Eqs. (11) to (14), the determinant of the matrix formed by the factors of the above four equations has to be zero.

Define

$$q=\frac{k_\mathrm{b}}{EI_\mathrm{eq}} \tag{15}$$

The equation for natural frequencies is

$$-\frac{q}{a}\cos aL\cosh aL+\sin aL\cosh aL-\cos aL\sinh aL-\frac{q}{a}=0 \tag{16}$$

The above equation does not have analytical solutions and is solved by numerical methods. The natural vibration mode corresponding to ω_n is

$$\phi_n(x)=A_1\sin a_nx+A_2\cos a_nx+A_3\sinh a_nx+A_4\cosh a_nx \tag{17}$$

The relationship of the four factors is derived by Eqs. (11) to (14) as follows:

$$A_2=-A_4 \tag{18}$$

$$A_3=A_4\frac{1+\cosh aL\cos aL-\sinh aL\sin aL}{\cosh aL\sin aL-\sinh aL\cos aL} \tag{19}$$

$$A_1=A_4\frac{1+\cos aL\cosh aL+\sin aL\sinh aL}{\cosh aL\sin aL-\sinh aL\cos aL} \tag{20}$$

The external static force s_n is[25]

$$s_n=\Gamma_n\boldsymbol{m}\boldsymbol{\phi}_n \tag{21}$$

where Γ_n is the modal participation factor; $\boldsymbol{m}$ is the mass matrix and $\boldsymbol{\phi}_n$ represents the natural mode of the n-th mode, which is represented by the continuous function $\phi_n(x)$ in this paper.

The static displacement and static inner forces including the bending moment, the shear and the rotation of each beam section under $\boldsymbol{s}_n$ can be derived based on the natural vibration frequencies and modes calculated.

The static displacement is

$$u_n^\mathrm{st}=\frac{\Gamma_n}{\omega_n^2}\phi_n=\frac{\Gamma_n}{\omega_n^2}(A_1\sin a_nx+A_2\cos a_nx+A_3\sinh a_nx+A_4\cosh a_nx) \tag{22}$$

The static bending moment in the wall is

$$M_\mathrm{w}^\mathrm{st}=EI\frac{\mathrm{d}^2u_n^\mathrm{st}}{\mathrm{d}x^2}=EI\frac{\Gamma_n}{\omega_n^2}(-A_1a_n^2\sin a_nx-A_2a_n^2\cos a_nx+A_3a_n^2\sinh a_nx+A_4a_n^2\cosh a_nx) \tag{23}$$

The static shear in the wall can be expressed as

$$V_\mathrm{w}^\mathrm{st}=EI\frac{\mathrm{d}^3u_n^\mathrm{st}}{\mathrm{d}x^3}=EI\frac{\Gamma_n}{\omega_n^2}(-A_1a_n^3\cos a_nx+A_2a_n^3\sin a_nx+A_3a_n^3\cosh a_nx+A_4a_n^3\sinh a_nx) \tag{24}$$

The rotation of each wall section is

$$\theta = \frac{\mathrm{d}u_n^{\mathrm{st}}}{\mathrm{d}x} = \frac{\Gamma_n}{\omega_n^2}(A_1 a_n \cos a_n x - A_2 a_n \sin a_n x + A_3 a_n \cosh a_n x + A_4 a_n \sinh a_n x) \tag{25}$$

After the BRBs yield, the rotational stiffness of the rotational spring is almost 0.02 times that of the elastic rotational stiffness. The first modal circular frequency is nearly zero as the simplified model is almost a pinned base beam.

Inner forces distribution in the HWBB-hinged frame after BRBs yield is illustrated in section 2.1.

1.2 HWBB-MRF

The simplified model of the HWBB-MRF structure is shown in Fig. 2. MRF is simplified as a shear beam with its lateral stiffness denoted as K (the shear force corresponding to unit interstory drift ratio). HWBB and MRF are connected through pinned links which can transfer the horizontal forces between those two systems. The relative stiffness of the moment resisting frame and the hinged wall is defined as the relative stiffness ratio λ[15].

$$\lambda = H\sqrt{\frac{K}{EI}} \tag{26}$$

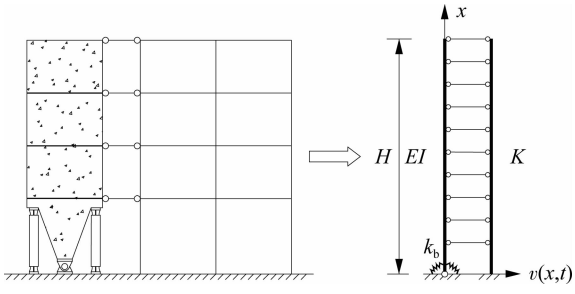

Fig. 2 The simplified model of the HWBB-MRF structure

The vibration equation of the simplified model of HWBB-MRF is[15]

$$EI\frac{\partial^4 v(x,t)}{\partial x^4} - K\frac{\partial^2 v(x,t)}{\partial x^2} + \bar{m}\frac{\partial^2 v(x,t)}{\partial t^2} = 0 \tag{27}$$

The definitions of α and β which are related to natural frequencies from Wu et al.[15] are as follows:

$$2m^2 = \frac{K}{EI} \tag{28}$$

$$n^4 = \frac{\bar{m}\omega^2}{EI} \tag{29}$$

$$\alpha = \sqrt{\sqrt{m^4 + n^4} + m^2} \tag{30}$$

$$\beta = \sqrt{\sqrt{m^4 + n^4} - m^2} \tag{31}$$

The general solution of Eq. (27) is[15]

$$\phi(x) = C_1\cosh\alpha x + C_2\sinh\alpha x + C_3\cos\beta x + C_4\sin\beta x \tag{32}$$

The boundary conditions are as follows:

When $x = 0$, $M(x=0) = k_b\frac{\mathrm{d}v}{\mathrm{d}x}(x=0)$,

$$C_1\alpha^2 - \alpha k_b C_2 - C_3\beta^2 - C_4 k_b\beta = 0 \tag{33}$$

When $x = 0$, $\phi(0) = 0$,

$$C_1 + C_3 = 0 \tag{34}$$

When $x = H$, $M = 0$,

$$C_1\alpha^2\cosh\alpha H + C_2\alpha^2\sinh\alpha H - C_3\beta^2\cos\beta H - C_4\beta^2\sin\beta H = 0 \tag{35}$$

When $x = H$, $V = K\frac{\mathrm{d}v(x)}{\mathrm{d}x} - EI\frac{\mathrm{d}^2 v(x)}{\mathrm{d}x^2} = 0$,

$$(K\alpha - EI\alpha^3)C_1\sinh\alpha H + (K\alpha - EI\alpha^3)C_2\cosh\alpha H - (K\beta + EI\beta^3)C_3\sin\beta H + (K\beta + EI\beta^3)C_4\cos\beta H = 0 \tag{36}$$

The frequency equation can be expressed as

$$\begin{aligned}&\alpha k_b\beta^2(K\beta + EI\beta^3) - k_b\beta\alpha^2(K\alpha - EI\alpha^3) + \\ &\sinh\alpha H\cos\beta H\alpha^2(K\beta + E\beta^3)(\alpha^2 + \beta^2) + \\ &\sin\beta H\cosh\alpha H\beta^2(K\alpha - EI\alpha^3)(\alpha^2 + \beta^2) + \\ &\sinh\alpha H\sin\beta H[k_b\beta\alpha^2(K\beta + EI\beta^3) + \\ &\alpha k_b\beta^2(K\alpha - EI\alpha^3)] + \cos\beta H\cosh\alpha H\cdot \\ &[-k_b\beta^3(K\alpha - EI\alpha^3) + \alpha^3 k_b(K\beta + EI\beta^3)] = 0\end{aligned} \tag{37}$$

An analytical solution cannot be obtained from this equation but numerical solutions can be obtained.

The natural vibration mode corresponding to ω_n is

$$\phi_n(x) = C_1\cosh\alpha_n x + C_2\sinh\alpha_n x + C_3\cos\beta_n x + C_4\sin\beta_n x \tag{38}$$

where

$$C_2 = C_1\frac{EI(\alpha^2 + \beta^2)\beta\sin\beta H - k_b(\alpha^2\cosh\alpha H + \beta^2\cos\beta H)}{\alpha(k_b\beta\sin\beta H + k_b\alpha\sinh\alpha H)} \tag{39}$$

$$C_3 = -C_1 \tag{40}$$

$$C_4 = \frac{1}{\beta}\left[C_1\frac{EI(\alpha^2 + \beta^2)}{k_b} - C_2\alpha\right] \tag{41}$$

Based on the natural vibration frequencies and modes calculated, the static displacement and inner forces can be derived as

$$u_n^{\mathrm{st}} = \frac{\Gamma_n}{\omega_n^2}\phi_n(x) = \frac{\Gamma_n}{\omega_n^2}(C_1\cosh\alpha_n x + C_2\sinh\alpha_n x + C_3\cos\beta_n x + C_4\sin\beta_n x) \tag{42}$$

$$M_{\mathrm{w}}^{\mathrm{st}} = EI\frac{\mathrm{d}^2 u_n^{\mathrm{st}}}{\mathrm{d}x^2} = EI\frac{\Gamma_n}{\omega_n^2}(C_1\alpha_n^2\cosh\alpha_n x + C_2\alpha_n^2\sinh\alpha_n x - C_3\beta_n^2\cos\beta_n x - C_4\beta_n^2\sin\beta_n x) \quad (43)$$

$$M_{\mathrm{f}}^{\mathrm{st}} = \int_x^H V_{\mathrm{f}}(\xi)\,\mathrm{d}\xi = \int_x^H K\frac{\Gamma_n}{\omega_n^2}(C_1\alpha_n\sinh(\alpha_n\xi) + C_2\alpha_n\cosh(\alpha_n\xi) - C_3\beta_{\mathrm{n}}\sin(\beta_n\xi) + C_4\beta_n\cos(\beta_n\xi))\,\mathrm{d}\xi \quad (44)$$

$$M_{\mathrm{t}}^{\mathrm{st}} = M_{\mathrm{f}}^{\mathrm{st}} + M_{\mathrm{w}}^{\mathrm{st}} \quad (45)$$

where $M_{\mathrm{t}}^{\mathrm{st}}$ is the total bending moment of the structure, $M_{\mathrm{f}}^{\mathrm{st}}$ represents the bending moment in the MRF and $M_{\mathrm{w}}^{\mathrm{st}}$ represents the bending moment in the wall of the HWBB.

$$V_{\mathrm{f}}^{\mathrm{st}} = K\theta = K\frac{\Gamma_n}{\omega_n^2}(C_1\alpha_n\sinh\alpha_n x + C_2\alpha_n\cosh\alpha_n x - C_3\beta_n\sin\beta_n x + C_4\beta_n\cos\beta_n x) \quad (46)$$

$$V_{\mathrm{t}}^{st} = \int_x^H s_n(\xi)\,\mathrm{d}\xi = \int_x^H \Gamma_n m(C_1\cosh\alpha_n\xi + C_2\sinh\alpha_n\xi + C_3\cos\beta_n\xi + C_4\sin\beta_n\xi)\,\mathrm{d}\xi \quad (47)$$

$$V_{\mathrm{w}}^{\mathrm{st}} = V_{\mathrm{t}}^{\mathrm{st}} - V_{\mathrm{f}}^{\mathrm{st}} \quad (48)$$

where $V_{\mathrm{t}}^{\mathrm{st}}$ is the total shear borne by the structure caused by the external force s_n; $V_{\mathrm{f}}^{\mathrm{st}}$ is the shear in the MRF; and $V_{\mathrm{w}}^{\mathrm{st}}$ is the shear in the hinged wall.

The response spectrum analysis method in Ref. [25] is used to calculate dynamic responses by multiplying the modal static responses to the pseudo acceleration corresponding to each modal period. The SRSS method can be used to combine different modal reactions according to the Chinese seismic code for structures with well-separated natural frequencies[26].

The HWBB can be simplified as a hinged wall due to the small post-yielding stiffness of BRBs. For the HWBB-hinged frame structure, the first modal period after BRBs yield is larger than 15 s due to the small post yielding stiffness of BRB. Therefore, the pseudo acceleration of the first mode is almost zero[25]. The first mode will no longer contribute to the inner forces. Higher modes have to be considered after the yielding of BRB. This is illustrated by the example in section 2.1. As displacement is not sensitive to higher modes, the whole displacement varies linearly along the height of the structure and is controlled by the first mode after the BRBs yield. For the HWBB-MRF structure, the MRF still provides the lateral stiffness for the whole structure after the BRBs yield and the first mode contribute to the inner forces after the BRBs yield[15].

2 Example Models

In this section, example models contain both the HWBB-hinged frame and HWBB-MRF. Pseudo-accelerations corresponding to different modal periods are obtained according to the design spectrum in Chinese seismic design code for frequent earthquakes with intensity 7.

2.1 HWBB-hinged frame structure

The prototype building is a twelve-story structure accompanied by two HWBBs in each direction of the building, with uniform properties over the height. Fig. 3(a) depicts the floor plan, which has a footprint of 23.6 m × 50.4 m with 4.0-m story heights. Concrete with 40 MPa nominal compression strength is used. Due to the symmetricity of the structure, a half structure is modeled. The seismic weight of each half of the building is 6 800 kN at each floor level. As shown in Fig. 3(b), the cross section of the wall is 0.35 m × 8.4 m and the flexural stiffness of the wall is $EI = 562$ GN · m^2. The area of the core plate of BRB is 22 000 mm^2, the length of BRB is 3.7 m, and the distance between centerlines of two BRBs is 8.1 m, resulting in $k_{\mathrm{b}} = 40$ GN · m. The frame in the prototype building bears only a vertical load and belongs to a hinged frame which does not have any lateral resistance. The first three natural periods of this structure are 3.36, 0.452 and 0.151 s, respectively. The first three natural vibration modes are shown in Fig. 4.

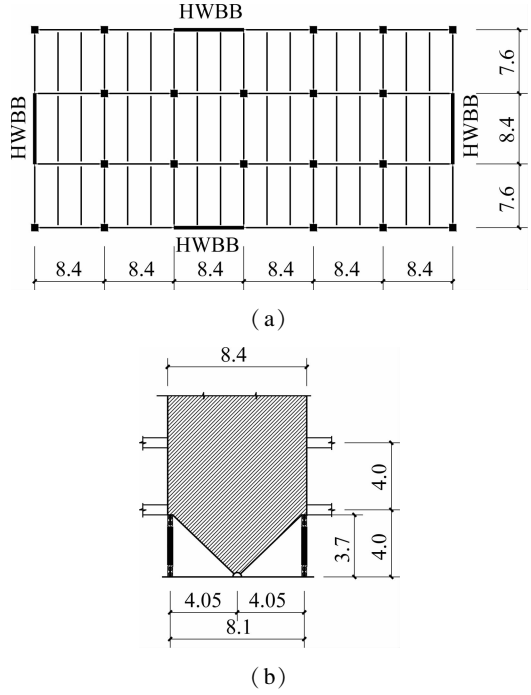

Fig. 3 Structural layout of the numerical example (unit: m). (a) Plan view; (b) Detail of HWBB

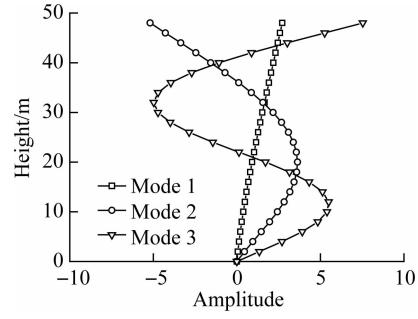

Fig. 4 Natural modes of the HWBB-hinged frame

Fig. 5(a) depicts the static displacement in the HWBB corresponding to the first three modes. The maximum static displacement corresponding to mode 1 is 100 times that of mode 2 and 1 600 times that of mode 3, indicating that the first mode is dominant. Fig. 5(b) depicts the dynamic displacement in the HWBB along the height. The total displacement is predominantly controlled by the first mode as the maximum dynamic displacement of the first mode is 99.86% times that of the SRSS result, while contributions from the second and third modes are 4.15% and 0.283% times that of the SRSS result, respectively. It can be seen from Fig. 5(c) and Fig. 5(d) that higher modes have to be considered for shear and bending moment design in the HWBB. In Fig. 5(c), the maximum shear in mode 1 is 65.9% that of SRSS, while the maximum shears in mode 2 and mode 3 are 71.49% and 23.3% that of SRSS, respectively. In Fig. 5(d), the maximum moment in mode 1 is 98.7% that of SRSS, and the maximum moments in mode 2 and mode 3 are 30.24% and 6.31% that of SRSS, respectively.

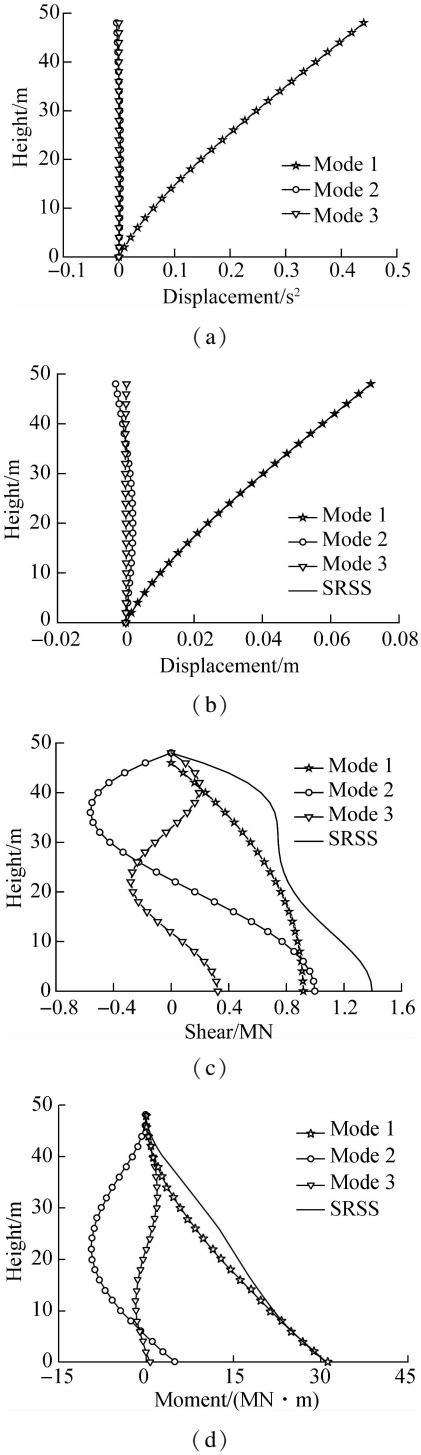

Fig. 5 Responses of HWBB. (a) Static displacement; (b) Dynamic displacement; (c) Shear in HWBB; (d) Moment in HWBB

Fig. 6 is the inner forces distribution in the HWBB after the BRBs yield. Due to the fact that the pseudo acceleration corresponding to the first mode almost equals zero, the first mode does not contribute to the inner forces. In Fig. 6(a), the maximum shear in mode 2 is 93% that of SRSS, while the maximum shears in mode 3 and mode 4 are 33.3% and 14.4% that of SRSS, respectively. In Fig. 6(b), the maximum moment in mode 2 is 98% that of SRSS, while the maximum moments in mode 3 and mode 4 are 20.5% and 6% that of SRSS, respectively. It indicates that higher modes have to be considered in the calculation of inner forces in HWBB after the BRBs yield.

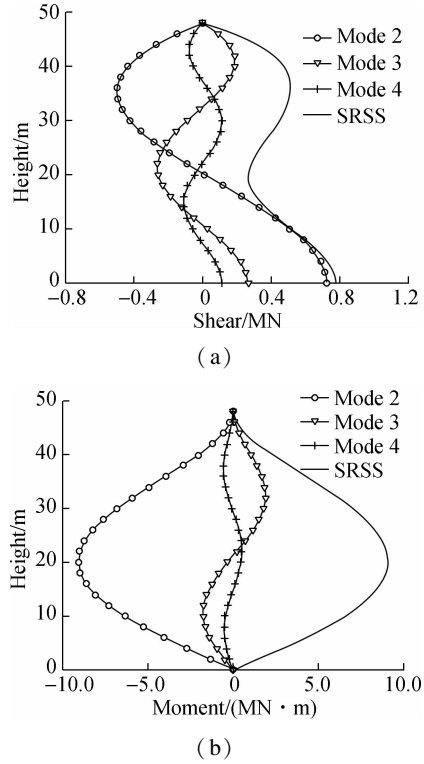

Fig. 6 Response of HWBB after BRBs yield. (a) Shear in HWBB; (b) Moment in HWBB

2.2 HWBB-MRF

The properties and dimensions of the HWBB are the same as the HWBB-hinged frame structure in section 2.1. The shear stiffness of the MRF is 549 MN, which corresponds to a relative stiffness ratio of 1.5. The first

three natural periods are 1.69, 0.34 and 0.13 s, respectively. The natural mode shapes of the first three modes are shown in Fig. 7.

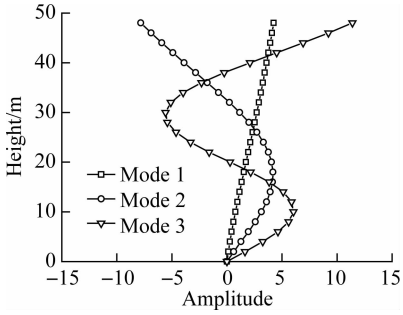

Fig. 7 Natural mode shapes of the first three modes

2.2.1 Equivalent static response

The equivalent static displacement is dominantly controlled by the first mode, as shown in Fig. 8.

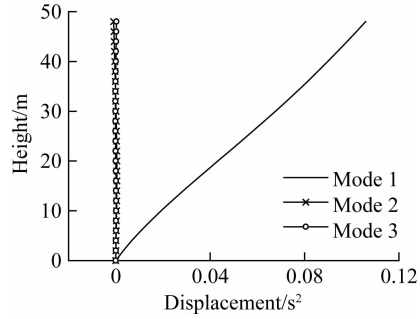

Fig. 8 Static displacement distribution for the first three modes

The shear distribution is depicted in Fig. 9. In mode 1, both the contributions from the wall and the frame have to be considered since the maximum shear of the structure is 4.38 and 1.16 times those of the frame and HWBB. The shear borne by the MRF significantly decreases in mode 2 and mode 3.

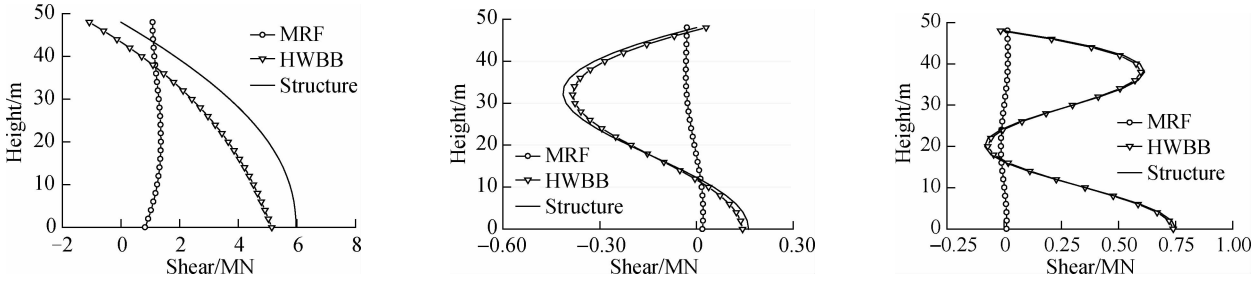

Fig. 9 Shear distribution for the first three modes. (a) Mode 1; (b) Mode 2; (c) Mode 3

Fig. 10 depicts the bending moment distribution. The contribution from the frame decreases sharply as the mode increases, especially for mode 3. The contributions from the wall are 4.514 and 10.99 times those of the frame in mode 2 and mode 3, respectively.

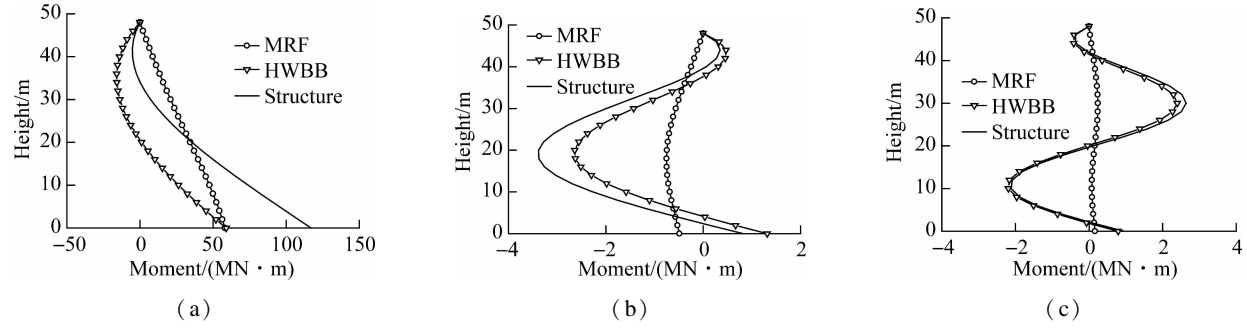

Fig. 10 Bending moment distribution for the first three modes. (a) Mode 1; (b) Mode 2; (c) Mode 3

The static displacement is dominated by the first mode, and the frame contributes little to the shear and moment distribution in higher modes (mode 2 and mode 3). However, the wall contributes predominantly to the shear and moment in higher modes.

2.2.2 Dynamic response

Fig. 11 depicts dynamic responses, which include the displacement and inner forces. Displacement is controlled by the first mode. Fig. 11(a) depicts the shear in the frame. It can be seen that higher mode effects are not significant in the frame because HWBB can effectively control the deformation pattern of the frame. Therefore, the shear demand of the frame can be estimated only based on the first mode. Fig. 11(a) indicates that the shear corresponding to the first mode is 99.9% that of SRSS and the shears for mode 2 and mode 3 are 8.79% and 4.62% that of SRSS, respectively.

Fig. 11(b) depicts the dynamic displacement response. It can be seen from the figure that the SRSS value is almost identical to the displacement of the first mode. This indicates that mode 2 and mode 3 can be ignored and mode 1 can be used to estimate the displacement demand.

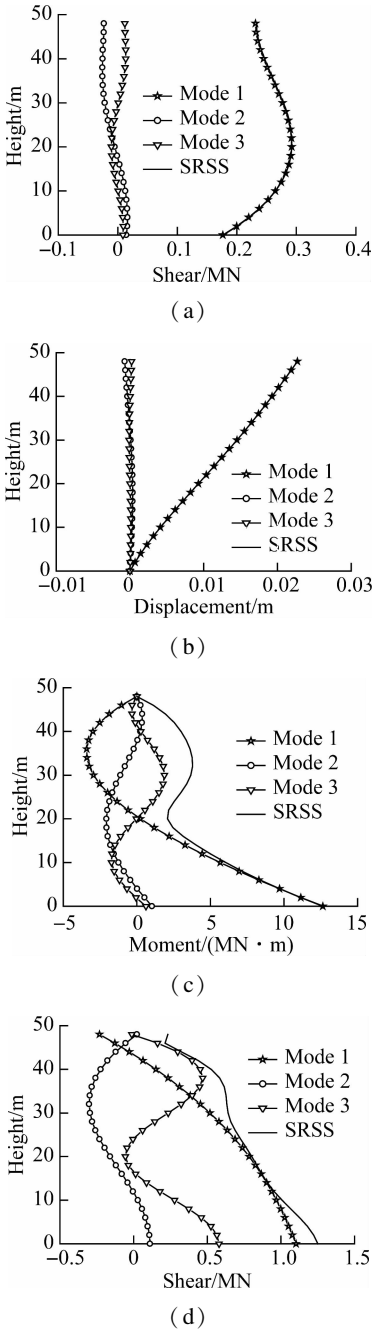

Fig. 11 Dynamic response. (a) Shear in the frame; (b) Displacement; (c) Bending moment in HWBB; (d) Shear in HWBB

Fig. 11(c) illustrates the bending moment distribution in HWBB. The maximum moment of mode 1 is 99.55% that of the SRSS, and the maximum moments of mode 2 and mode 3 are 16.29% and 14.79% that of the SRSS, respectively. This indicates that higher modes have a non-negligible effect on the bending moment distribution of the wall and need to be considered when determining the bending moment demand of the wall. Fig. 11(d) is the shear in the hinged wall. The maximum shear of the first mode in the wall is 99.55% that obtained using the SRSS method, and the maximum values of mode 2 and mode 3 are 16.29% and 14.79% that of SRSS, respectively. This indicates that higher mode effects have to be considered when determining the shear demand in the wall.

From the above analysis, it can be seen that higher modes have a remarkable effect on the inner force distribution in the wall. Therefore, higher mode effects have to be considered during the strength design of the wall. However, the displacement and shear force in the frame are controlled by the first mode, which demonstrates that HWBB has effectively controlled the deformation pattern of the MRF.

3 Parameter Analysis

In this section, the effect on the seismic performance of two parameters, which are the relative stiffness ratio and the rotational stiffness ratio, are analyzed.

3.1 Relative stiffness ratio

The model in section 2.2 is used in the analysis. The variation of the relative stiffness ratio is realized by the variation of the flexural stiffness of the wall, while the lateral stiffness of MRF remains constant. The effect of the relative stiffness ratio on the modal shape is illustrated in Fig. 12. With the decrease in the relative stiffness ratio, the flexural stiffness of the wall increases, and the displacement amplitude corresponding to each mode decreases. The flexural stiffness of the wall reduces the displacement amplitude of mode shapes corresponding to the first three modes. However, after the relative stiffness ratio reaches a certain value, the increase in the flexural stiffness will neither effectively reduce the displacement of the mode shape nor be cost-effective.

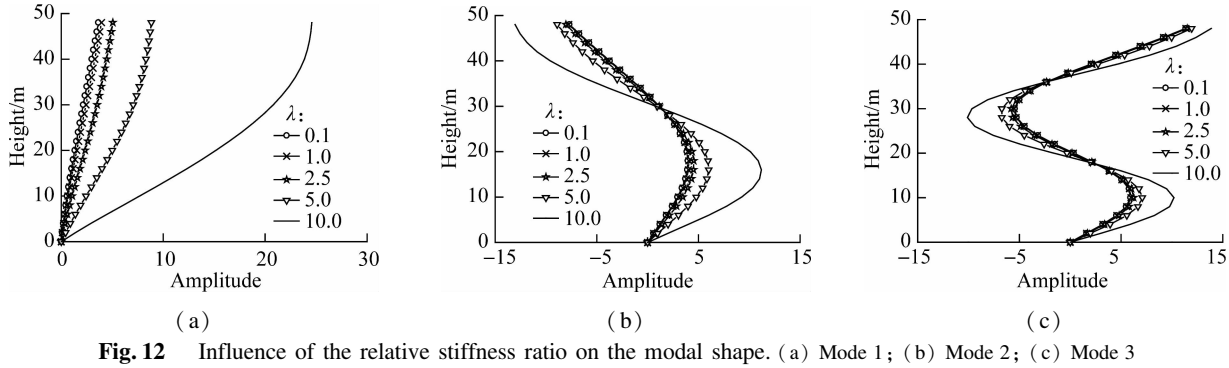

Fig. 12 Influence of the relative stiffness ratio on the modal shape. (a) Mode 1; (b) Mode 2; (c) Mode 3

Fig. 13 presents the cumulative effective modal mass ratio of the first three modes. The minimum value corresponding to the first mode is larger than 70%, and the contribution from the third mode is larger than the contribution from the second mode. The effective modal mass corresponding to the first mode and second mode increases with the increase in the relative stiffness ratio, while the effective modal mass of the third mode decreases with the increase of relative stiffness. When the relative stiffness ratio is larger than or equal to 10, the cumulative effective modal mass of the first three modes will be larger than 90%, which can meet the requirement of the seismic code[26] for the minimum number of modes needed to be considered in analysis.

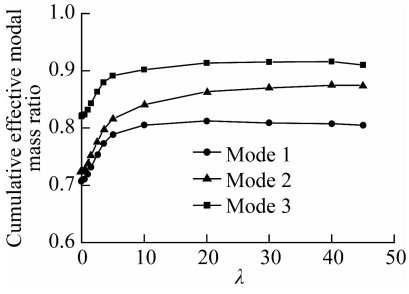

Fig. 13 Influence of the relative stiffness ratio on the cumulative effective modal mass ratio of the first three modes

3.2 Relative stiffness of the hinged wall and rotational spring

The rotational stiffness ratio, which is the relative stiffness ratio of the rotational stiffness of the rotational spring and the flexural stiffness of the wall, is as follows:

$$\beta = \frac{k_b h}{EI} \tag{49}$$

where h is the story height, which is assumed to be the same along the height of the building for brevity.

To investigate the effect of the rotational stiffness ratio, the model used is the HWBB-hinged frame structure in section 2.1. The variation of the rotational stiffness ratio is realized by the variation of the rotational stiffness of the rotational spring, while the flexural stiffness of the wall remains constant. The rotational stiffness ratio for the HWBB-hinged frame structure in section 2.1 is 0.28. Fig. 14 demonstrates the effect of the rotational stiffness ratio on frequencies. The first three periods decrease with the increase in the rotational stiffness ratio. However, when the rotational stiffness becomes infinitesimal, HWBB tends towards a pin-supported wall. When the rotational stiffness becomes large enough, HWBB tends towards a cantilever beam. This is the reason why frequencies no longer vary when the rotational stiffness ratio is either too small or too large, as seen from the two flat lines in each figure.

The base shear modal contribution factor corresponding to mode n is[25]

$$\psi_n = \frac{M_n^*}{\bar{m}H} = \frac{V_{bn}^{st}}{\sum_{n=1}^{N} V_{bn}^{st}} \tag{50}$$

where N denotes the total number of modes and M_n^* denotes the base shear effective modal mass corresponding to mode n.

The effective modal mass is the contribution of each mode to the static base shear. As illustrated in Fig. 15,

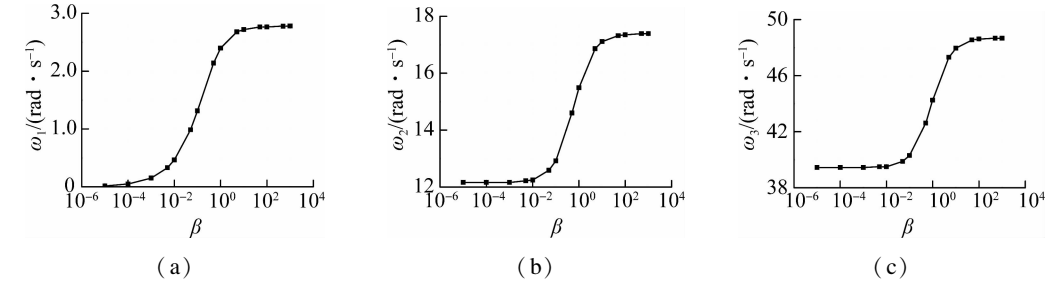

Fig. 14 Influence of the rotational stiffness ratio on the natural frequencies. (a) Mode 1; (b) Mode 2; (c) Mode 3

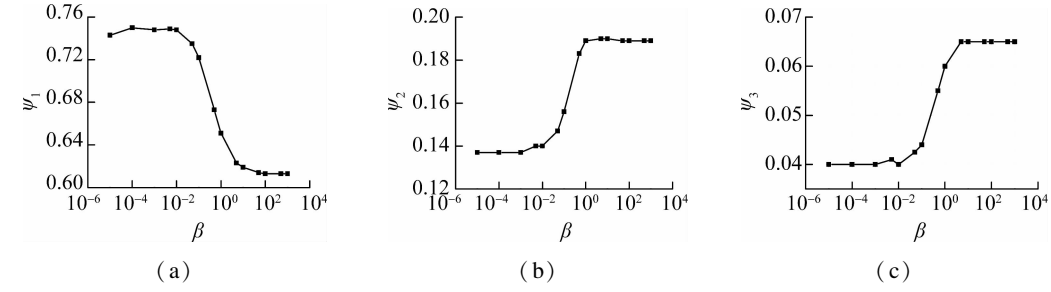

Fig. 15 Influence of the rotational stiffness ratio on the effective modal mass. (a) Mode 1; (b) Mode 2; (c) Mode 3

the first mode effective mass decreases with the increase in the rotational stiffness ratio, while the second and third modes increase with the increase in the rotational stiffness ratio. The sum of the first three modes decreases with the increase in the rotational stiffness ratio. With the increase in the relative stiffness ratio, higher modes become more important in the contribution of the base shear.

4 Conclusions

1) Vibration equations are derived to investigate higher mode effects in the HWBB-frame structure. Modal analysis of the simplified models of both the HWBB-hinged frame and HWBB-MRF has been derived. Natural vibration periods and modes are derived accordingly.

2) Higher modes can influence the bending moment and shear distribution in the hinged wall, while they can be ignored in the shear distribution in MRF, which is due to the controlling function of HWBB. Moreover, the global displacement is also controlled by the fundamental mode.

3) For the HWBB-hinged frame structure, after the BRBs yield, the displacement of the HWBB-hinged frame is also controlled by the first mode. Therefore, displacement is not sensitive to higher modes. However, the first mode will no longer contribute to the inner forces. Higher modes have to be considered when determining the inner forces demand after the BRBs yield. For the HWBB-MRF structure, the first mode contributes to inner forces after the BRBs yield as MRF provides the lateral stiffness for the whole structure after the BRBs yield.

4) Parameter analysis demonstrates that the increase in the flexural stiffness wall can decrease the displacement amplitudes of the first three modes. However, after the flexural stiffness reaches a certain value, the displacement amplitude varies slowly. The first three periods all decrease with the increase in the rotational stiffness, which demonstrates that the rotational stiffness of the rotational spring can enlarge the stiffness of HWBB. With the increase in the rotational stiffness ratio, the contribution from the first mode decreases, and contributions from both the second mode and third mode increase.

References

[1] Alavi B, Krawinkler H. Strengthening of moment-resisting frame structures against near-fault ground motion effects [J]. *Earthquake Engineering and Structural Dynamics*, 2004, **33**(6): 707 – 722. DOI: 10. 1002/eqe. 370.

[2] Wada A, Qu Z, Ito H, et al. Seismic retrofit using rocking walls and steel dampers [C]//*ATC and SEI Conference on Improving the Seismic Performance of Existing Buildings and Other Structures*. San Francisco, USA, 2009: 1010 – 1021.

[3] Wada A, Qu Z, Sakata H. Seismic retrofit of existing SRC frames using rocking walls and steel dampers [J]. *Frontiers of Architecture and Civil Engineering in China*, 2011, **5**(3): 259 – 266. DOI: 10. 1007/s11709-011-0114-x. (in Chinese)

[4] Qu Z, Wada A, Motoyui S, et al. Pin-supported walls for enhancing the seismic performance of building structures [J]. *Earthquake Engineering and Structural Dynamics*, 2012, **41**(14): 2075 – 2091. DOI: 10. 1002/eqe. 2175.

[5] Janhunen B, Tipping S, Mar T. Seismic retrofit of a 1960s steel moment-frame highrise using a pivoting spine [C]//*Proceedings of the Structural Engineering Association of California* 82*nd Annual Convention*. San Diego, USA, 2013: 320 – 336.

[6] Makris N, Aghagholizadeh M. The dynamics of an elastic structure coupled with a rocking wall [J]. *Earthquake Engineering and Structural Dynamics*, 2017, **46**(6): 945 – 962. DOI: 10. 1002/eqe. 2838.

[7] Kurama Y, Sause R, Pessiki S. Lateral load behavior and seismic design of unbonded post-tensioned precast concrete walls [J]. *ACI Structural Journal*, 1999, **96**(4): 622 – 632. DOI: 10. 14359/700.

[8] Takeuchi T, Suzuki K. Performance-based design for truss-frame structures using energy dissipation devices [C]//*Proceedings of the* 4*th International Conference on Behavior of Steel Structures in Seismic Areas*. Naples, Italy, 2003: 55 – 61.

[9] Takeuchi T, Chen X, Matsui R. Seismic performance of controlled spine frames with energy-dissipating members [J]. *Journal of Constructional Steel Research*, 2015, **114**: 51 – 65. DOI: 10. 1016/j. jcsr. 2015. 07. 002.

[10] Chen X, Takeuchi T, Matsui R. Simplified design procedure for controlled spine frames with energy-dissipating members [J]. *Journal of Constructional Steel Research*, 2017, **135**: 242 – 252. DOI: 10. 1016/j. jcsr. 2017. 04. 017.

[11] Chen X, Takeuchi T, Matsui R. Seismic performance and evaluation of controlled spine frames applied in high-rise buildings [J]. *Earthquake Spectra*, 2018, **34**(3): 1431 – 1458. DOI: 10. 1193/080817eqs157m.

[12] Djojo G S, Clifton G C, Henry R S, et al. Experimental testing of a double acting ring spring system for use in rocking steel shear walls [C]//8*th International Conference on Behavior of Steel Structures in Seismic Areas*. Shanghai, China, 2015: 1245 – 1252.

[13] Du Y F, Wu D Y. Performance analysis of light energy dissipative rocking frame designed on the basis of stiffness demand [J]. *China Civil Engineering Journal*, 2014, **47**(1): 24 – 35. DOI: 10. 15951/j. tmgcxb. 2014. 01. 006. (in Chinese)

[14] Wiebe L, Christopoulos C. Mitigation of higher mode effects in base-rocking systems by using multiple rocking sections[J]. *Journal of Earthquake Engineering*, 2009, **13**(sup1): 83 – 108. DOI: 10. 1080/13632460902813315.

[15] Wu S J, Pan P, Zhang D B. Higher mode effects in frame pin-supported wall structure by using a distributed model [J]. *Earthquake Engineering and Structural Dynamics*, 2016, **45**(14): 2371 – 2387. DOI: 10. 1002/eqe. 2766.

[16] Grigorian C E, Grigorian M. Performance control and efficient design of rocking-wall moment frames[J]. *Jour-*

nal of Structural Engineering, 2016, **142**(2): 04015139. DOI:10.1061/(asce)st.1943-541x.0001411.

[17] Grigorian M, Grigorian C. An introduction to the structural design of rocking wall-frames with a view to collapse prevention, self-alignment and repairability [J]. *The Structural Design of Tall and Special Buildings*, 2016, **25**(2): 93－111. DOI:10.1002/tal.1230.

[18] Grigorian M, Grigorian C E. Sustainable earthquake-resisting system [J]. *Journal of Structural Engineering*, 2018, **144**(2): 04017199. DOI: 10.1061/(asce)st.1943-541x.0001900.

[19] Nima R, Moghadam A S, Aziminejad A. Continuum analysis approach for rocking core-moment frames [J]. *Journal of Structural Engineering*, 2018, **144**(3): 04018006. DOI: 10.1061/(asce)st.1943-541x.0001986.

[20] Wiebe L, Christopoulos C. A cantilever beam analogy for quantifying higher mode effects in multistorey buildings[J]. *Earthquake Engineering & Structural Dynamics*, 2015, **44**: 1697－1716. DOI:10.1002/eqe.2549.

[21] Yang X Y, Wu J, Zhang J, et al. Post-yielding behavior of hinge-supported wall with buckling-restrained braces in base [J]. *Journal of Earthquake and Tsunami*, 2019, **13**(3/4): 1940003. DOI:10.1142/s1793431119400037.

[22] Wang X T, Wang T, Qu Z. An experimental study of a damage-controllable plastic hinge-supported wall structure [J]. *Earthquake Engineering and Structural Dynamics*, 2018, **47**(3): 594－612. DOI:10.1002/eqe.2981.

[23] Yang X Y, Feng Y L, Wu J, et al. Experimental study on seismic performance of hinged truss with buckling-restrained braces at base [J]. *Journal of Southeast University (Natural Science Edition)*, 2018, **48**(2): 303－309. (in Chinese)

[24] Clough R W, Penzien J. *Dynamics of structures*[M]. 3rd eds. Berkeley, CA, USA: Computer & Structures, Inc, 1995.

[25] Chopra A K. *Dynamics of structures: Theory and applications to earthquake engineering*[M]. Upper Saddle River, NJ, USA: Prentice Hall, 2007.

[26] Ministry of Housing and Urban-Rural Development of the People's Republic of China. GB 50011—2010 Code for seismic design of Buildings [S]. Beijing: China Architecture and Building Press, 2010. (in Chinese)

采用分布参数模型考虑高阶模态对底部带 BRBs 的铰支墙-框架结构的影响

杨晓燕[1] 吴 京[1] 庞熙熙[2] 王 强[3] 张 萌[4]

([1] 东南大学混凝土及预应力混凝土结构教育部重点实验室, 南京 211189)

([2] 国网经济技术研究院有限公司徐州勘测设计中心, 徐州 221005)

([3] 香港华艺设计顾问(深圳)有限公司, 深圳 518057)

([4] 宝胜系统集成科技股份有限公司, 宝应 225000)

摘要:为了研究高阶模态对底部带 BRB 的铰支墙(HWBB)框架结构的影响,建立了 HWBB-铰接框架和 HWBB-抗弯框架的分布参数模型. 将铰支墙简化为弯曲梁、BRB 简化为转角弹簧、抗弯框架简化为剪切梁. 推导出 2 种分布参数模型的振动方程,求出各阶周期、各个振型及内力和位移的数值解. 研究了相对刚度比以及转动刚度比对高阶模态效应的影响. 对于弹性结构,整体位移及抗弯框架中的剪力由一阶模态控制,而墙中的剪力和弯矩受高阶模态影响较大. 同时研究了 BRB 屈服对 HWBB-铰接框架结构内力分布的影响. 结果表明:在 BRB 屈服后,原一阶模态将不再对内力产生贡献,而高阶模态对内力贡献作用将增加. 但 BRB 屈服后位移对高阶模态不敏感、仍由一阶模态控制. 参数分析表明:在墙的抗弯刚度达到一定值前,随着墙抗弯刚度的增加,结构的位移会逐渐减小;随着转动刚度的增加,前三阶周期会减小;随着转动刚度比的增加,一阶模态的基底剪力贡献系数减小,但二阶和三阶模态的基底剪力贡献系数增加.

关键词:铰支墙;高阶模态;弯曲梁;转动弹簧;转动刚度比

中图分类号:TU352.1